

RESEARCH

Open Access



An investigation on the solidification and porosity prediction in aluminium casting process

Samir Chakravarti^{1,2} and Swarnendu Sen^{1*}

*Correspondence:
sen.swarnendu@gmail.com

¹ Department of Mechanical Engineering, Jadavpur University, Kolkata, West Bengal 700032, India

² Department of Mechanical Engineering, Kalyani Government Engineering College, Kalyani, West Bengal 741235, India

Abstract

Air porosity becomes an issue in casting that needs attention. To create superior-quality castings, it is crucial to carefully consider the parameters of the casting for negligible air porosity. The manuscript presents a study of porosity with the filling and solidification process inside the mould cavity where flow is turbulent using a computational fluid dynamics (CFD) approach by Ansys Fluent. An Ansys Fluent simulation model has been created and validated using the existing experimental research. This model investigates the variation in solid aluminium (about 100% Al) filled from the base of the mould cavity as a function of pouring temperature and pouring velocity. The relationship between porosity and casting parameters has been investigated and it is used to forecast a better estimate for the casting parameters with minimum porosity. It is observed that the top surface of the casting, which is linked to the bottom surface of the riser, has the maximum porosity and when the pouring velocity is close to 500 mm/s, the porosity value is extremely low.

Keywords: Aluminium Casting, Casting Filling, Solidification, Porosity, Ansys fluent, Casting parameters, Filling thickness, Turbulent flow

Introduction

Aluminium (Al) and its alloys have recently received a lot of attention because of their extensive industrial applications and great technological value. The reason for its desirability is its advantageous properties, including low density, high thermal conductivity, exceptional corrosion resistance, high castability, and desirable tensile strength [1, 2]. It is therefore widely employed, particularly in the mechanical, automobile, and aerospace industries [1–3]. This article mainly concerns aluminium casting in a steel mould. While the casting solidifies, shrinkage porosity and gas or air porosity are the two main forms of porosity that arise.

Several works have explored the porosity arising during the solidification process in a variety of directions. Chudasama [4] used ProCAST software to analyse shrinkage porosity during metal filling and solidification for the gravity sand casting process. Ayar et al. [5] used the AutoCAST-X1 software to execute a casting simulation to examine the behaviour of molten filling and solidification and discovered a shrinkage porosity defect

in the centre feeder section. Naoya Hirata and Koichi Anzai [6] used the particle method of casting pure aluminium to examine the behaviour of shrinkage formation. Shrinkage porosity is expected to happen due to an advanced solidification of the liquid metal inside the riser and can be avoided by proper design and placement of the riser [7, 8].

On the other hand, some researchers claimed that air porosity is a common problem in aluminium castings since pores are usual occurrences in aluminium castings [9, 10]. The defects due to air porosity hamper their usage in safety-critical applications [3]. Porosity is expected to account for around 35% of overall defects in die-cast components [11]. A one-dimensional model has also been used to study porosity and temperature distribution [12, 13]. To calculate the air porosity to produce high-quality castings, it is also important to study the process of casting filling and solidification [14]. To design the casting simulation, inlet velocity, pouring temperature, and pouring time are important parameters [15, 16]. Choudhari et al. [8] stated the process of solidification in casting is complex and studied defects such as shrinkage cavity and porosity. Jolly and Katgerman [17] discussed how different defects arise during the solidification of shape and direct chill casting processes. Namchanchra et al. [18] investigated the stages of filling, solidification, and cooling during the manufacture of a plumbing component using the computational fluid dynamics (CFD) method. Nowadays, Ansys Fluent simulation software is versatile and is widely used for the simulation of casting [19–21]. Eyal and Yagoob [22] focused on the use of Ansys Fluent simulation software for numerical modelling of ZA alloy casting solidification.

Mozammil et al. [15] established that the pouring time is expected to play a significant role in the casting and this direction of research should be further pursued in the future. It was suggested that the pouring time should be fixed in such a way the mould cavity is properly filled before the solidification process begins [15, 23]. Some researchers assumed that the mould cavity is filled with molten metal as the beginning condition and neglected to analyse the casting process at the time when the mould is filled with molten metal [24].

Since the simulation of the casting process is complex, most of the researchers assumed that during the process, the solidification begins only after the total filling of molten metal in the mould cavity. In almost every state-of-the-art study, choosing the optimum pouring time is often regarded as a future direction of research. It is also observed that there is a research gap in the practical ideas about the solidification starting time and the pouring time. This implies that there is a need of choosing the appropriate parameters like pouring velocity, pouring temperature, and pouring time to ensure the highest percentage of aluminium filling in the mould cavity with negligible porosity.

This article aims to develop a more realistic simulation model in Ansys Fluent where it is expected that the solidification process may start from the beginning of the metal being poured; whereas the existing literatures [13, 15, 23, 24] invoked solidification after completion of the mould cavity filling process. The study is further extended to optimise pouring temperature and pouring velocity such that there is a higher percentage of aluminium filling in the mould cavity with minimum porosity. This work studies the mould filling and solidification of aluminium in the mould by presenting a two-phase system (air and aluminium) and a mixture of two phases with different states (liquid and solid) of aluminium. The model also predicts the location of porosity, variations in the

percentage of Al present throughout the casting thickness with casting parameters, and the region of maximum porosity. The present analysis also points out a novel overview of the variation in solid aluminium (about 100%) filled from the base of the mould cavity at different pouring parameters.

Methods

To simulate the casting process, Ansys Fluent [22] was employed. The metal filling and solidification model of transient flow gravity casting were studied by the two-phase volume of fluid method (VOF model) [18]. During the filling of the mould cavity, the molten metal enters the cavity through the inlet boundary of the sprue. The mould was initially filled with air at atmospheric temperature. During the pouring operation, the air in the cavity is permitted to leave through the riser's pressure outlet boundary. The process of filling a casting is a time-dependent flow of a viscous, incompressible liquid with a free surface. The RNG k- ϵ method has been used to model the turbulence inside the mould cavity [25, 26]. The RNG k-epsilon turbulence model is useful for predicting flow patterns in confined flow systems. Nzebuka et al. [21] and Waheed et al. [27] used the RNG k-epsilon turbulence model to investigate flow patterns and turbulent transport quantities in a horizontal direct-chill casting system. To reduce the casting time and extra metal loss, pouring time is measured as the ratio between the total volume (mould cavity, sprue, and riser) and the volume of molten metal entering per unit time through the inlet. Solidification is considered simultaneously with the metal pouring process. In this work, the casting process is studied by taking conjugate heat transmission and fluid flow phenomena into consideration. The mould has six outside boundary surface walls which are exposed to the atmosphere where natural convection occurs.

Solidification model

The numerical analysis of the casting solidification process taking into account the motions of the molten metal is dependent on the solution of the system of the following equations [18–22, 28, 29]: volume fraction equation, continuity equation, momentum equations, and energy equation.

The volume fraction of each phase throughout the domain can be monitored using the VOF model, which solves momentum equations. The properties in any cell are calculated for one of the phases or a combination of the phases based on the volume fraction of the various phases. The ratio of the occupied volume of a phase in a cell [m^3] to the total volume of the cell [m^3] defines the volume fraction of that phase in the cell.

In a two-phase system, subscripts a and b stand for the primary (air) and secondary (Al) phases, respectively, and their volume fractions are indicated as α_a and α_b in a particular cell. Then the following three possibilities exist in a given cell: $\alpha_b = 0$: the b^{th} phase is not present in the cell, $\alpha_b = 1$: the b^{th} phase fills the entire cell, and $0 < \alpha_b < 1$: both the phases are present and the interface between the b^{th} phase and a^{th} phase is present in the cell.

The interface(s) in a cell is measured between the phases by solving the volume fraction equation for the volume fraction of a single phase and the continuity equation. The volume fraction equation for the b^{th} phase has the following form:

$$\frac{\partial \alpha_b}{\partial t} + \vec{v} \cdot \nabla \alpha_b = 0 \quad (1)$$

where \vec{v} is the velocity vector and t is the time.

The continuity equation has the form:

$$\frac{\partial \rho}{\partial t} + \nabla(\rho \vec{v}) = 0 \quad (2)$$

where the density [kg m^{-3}] is denoted by ρ .

The total of the volume fractions of all phases in each cell (or control volume) equals one. Thus, the following formula is used to calculate the volume fraction values of the primary phase in a cell:

$$\alpha_a + \alpha_b = 1 \quad (3)$$

The volume fraction values of all phases govern the momentum equation through the properties of the mixture phase. Every mixture property is calculated in each cell using the volume fraction averaged approach, for instance, the density of a two-phase mixture in a cell is determined by

$$\rho = \alpha_a \rho_a + \alpha_b \rho_b = (1 - \alpha_b) \rho_a + \alpha_b \rho_b \quad (4)$$

In a cell, the property like thermal conductivity of Al is given by

$$K_{Al} = \beta K_l + (1 - \beta) K_s$$

where β is the liquid fraction of Al. The thermal conductivities of Al in liquid (K_l) and solid (K_s) phases are listed in Table 2.

The momentum equation takes on the form:

$$\frac{\partial(\rho \vec{v})}{\partial t} + \nabla(\rho \vec{v} \vec{v}) = -\nabla p + \rho \vec{g} + \nabla[\mu \nabla \vec{v}] + \frac{\partial(-\rho \overline{u_i' u_j'})}{\partial x_j} + \vec{F} \quad (5)$$

This is called Reynolds-averaged momentum equations with the velocities and other solution variables representing ensemble-averaged or time-averaged values. For the velocity component u at node i : $u_i = \overline{u}_i + u_i'$. Here, \overline{u}_i and u_i' are mean (ensemble-averaged) and fluctuating components of velocity and the term $-\rho \overline{u_i' u_j'}$ denotes Reynolds stress.

\vec{v} is the velocity vector [m/s], μ is the dynamic viscosity coefficient [$\text{kg m}^{-1} \text{s}^{-1}$], g is the gravitational acceleration [m s^{-2}], and F is the source term used to modify the momentum equations in the mushy region. Carman-Koseny [28] suggested the following form for the source term.

$$\vec{F} = -\frac{C_{\text{mush}} \vec{v} (1 - \beta)^2}{\beta^3 + \epsilon} \quad (6)$$

The C_{mush} is the mushy zone constant and a value of 0.001 is assigned to the constant ϵ to avoid division by zero.

Each cell in the domain has a quantity called the liquid fraction which represents the fraction of the cell volume that is in liquid form. The solidification process is simulated in Ansys Fluent using the enthalpy-porosity approach. The porosity in the solidified casting is measured by the ratio of the total volume of air present in the solidified casting to the total volume of the casting. The liquid fraction value is determined by solving an enthalpy balance equation for every iteration. The material enthalpy is determined as the sum of the sensible heat (h_1) and latent heat (h_2), as shown below:

$$h = h_1 + h_2 \quad (7)$$

$$h_1 = h_{\text{ref}} + T \int_{\text{ref}}^T C_p dT \quad (8)$$

where h is the total enthalpy [J]. The specific heat at constant pressure [$\text{J kg}^{-1} \text{K}^{-1}$] is denoted by C_p , the reference temperature [K] is T_{ref} , and h_{ref} represents the reference enthalpy [J].

The latent heat component can be represented in terms of the latent heat of the material, L [J], and liquid fraction, β .

$$h_2 = \beta L \quad (9)$$

The liquid fraction can be addressed as

$$\beta = \begin{cases} 0 & \text{if } T \leq T_S \\ \frac{T-T_S}{T_L-T_S} & \text{if } T_S < T < T_L \\ 1 & \text{if } T \geq T_L \end{cases} \quad (10)$$

Where T_S and T_L are the solidus and liquidus temperatures [K] of Al. The latent heat component (h_2) may vary from zero (for solids) to L (for liquids).

The equation of energy is written as

$$\frac{\partial(\rho E)}{\partial t} + \nabla(\vec{v}(\rho E + p)) = \nabla(k_{\text{eff}} \nabla T) + \nabla(\bar{\tau} \vec{v}) + S_h \quad (11)$$

$$E = h - \frac{p}{\rho} + \frac{v^2}{2}$$

$$k_{\text{eff}} = k + k_t$$

$$k_t = \frac{c_p \mu_t}{Pr_t}$$

The stress tensor $\bar{\tau} = \mu_{\text{eff}} \left(\frac{\partial \bar{u}_i}{\partial x_j} + \frac{\partial \bar{u}_j}{\partial x_i} \right)$

Where the total energy is denoted by E and the effective conductivity is denoted by k_{eff} . k_t , Pr_t , μ_t , and μ_{eff} are the turbulent thermal conductivity, turbulent Prandtl number, turbulent viscosity, and effective viscosity respectively. Energy transfer resulting from conduction and turbulence energy diffusion are represented by the first two terms on the right-hand side of the energy equation. S_h includes any volumetric heat sources. The

region where the liquid fraction is between 0 and 1 is known as the mushy zone. It is often modelled as a porous media, and when the material solidifies, the liquid fraction drops from 1 to 0. When a material is fully solid in a cell, the liquid fraction of the material is zero and the velocity drops to zero.

The RNG model presents equations for turbulent kinetic energy (k) and dissipation rate (ε) as follows.

$$\frac{\partial(\rho k)}{\partial t} + \nabla(\rho k \vec{v}) = \nabla(\alpha_k \mu_{eff} \nabla k) + G_k + G_b - \rho \varepsilon \quad (12)$$

$$\frac{\partial(\rho \varepsilon)}{\partial t} + \nabla(\rho \varepsilon \vec{v}) = \nabla(\alpha_k \mu_{eff} \nabla \varepsilon) + C_{\varepsilon 1} \frac{\varepsilon}{k} (G_k + C_{\varepsilon 2} G_b) - C_{\varepsilon 2} \rho \frac{\varepsilon^2}{k} \quad (13)$$

where, the turbulence kinetic energy generated by mean velocity gradients and buoyancy are represented by G_k and G_b , respectively. $C_{\varepsilon 1}$ and $C_{\varepsilon 2}$ are constants that are 1.42 and 1.68 respectively [28].

The G_k and G_b are written as follows:

$$G_k = -\rho \overline{u_i u_j} \frac{\partial u_j}{\partial x_i}$$

$$G_b = -g_i \frac{\mu_t}{Pr_t \mu} \frac{\partial p}{\partial x_i}$$

The system of all equations is solved by taking proper initial and boundary conditions using the Ansys Fluent [28].

Validation of the methods

For validation, the proposed method/model is compared with the experimental result of Mozammil et al. [15]. They have considered a bottom gated mould cavity for a plate measuring 100 mm × 50 mm × 25 mm and a bar 40 mm × 13 mm × 13 mm, as shown in Fig. 1. For aluminium casting, the green sand mould was used. Dimensions of several components employed in the bottom gating casting are shown in Table 1. They carried out experiments as well as simulations to find out porosity at different temperatures. Laminar flow was assumed by Mozammil et al. [15] for their simulation.

The same mould geometry has been considered for the validation work. The casting process has been simulated by our proposed methods/model for various pouring temperatures. A total of 153,101 quadrilateral elements were taken in the aluminium casting with sand mould. The mesh view is shown in Fig. 2. The thermophysical properties of aluminium and sand are taken from existing literature [30, 31]. The boundary conditions are imposed depending on the mould geometry.

Figure 3 shows the porosity value obtained from the simulation and experimental results of Mozammil et al. [15] at various pouring temperatures. At about 970 K, 1000 K, 1050 K, and 1075 K pouring temperatures the porosity from the experimental result of Mozammil et al. [15] are 0.0078, 0.0087, 0.0091, and 0.0095 while their simulation result of porosity yields values of 0.0073, 0.0076, 0.0082, and 0.0085 respectively. The porosity obtained by the present study's simulation result following the use of our model is

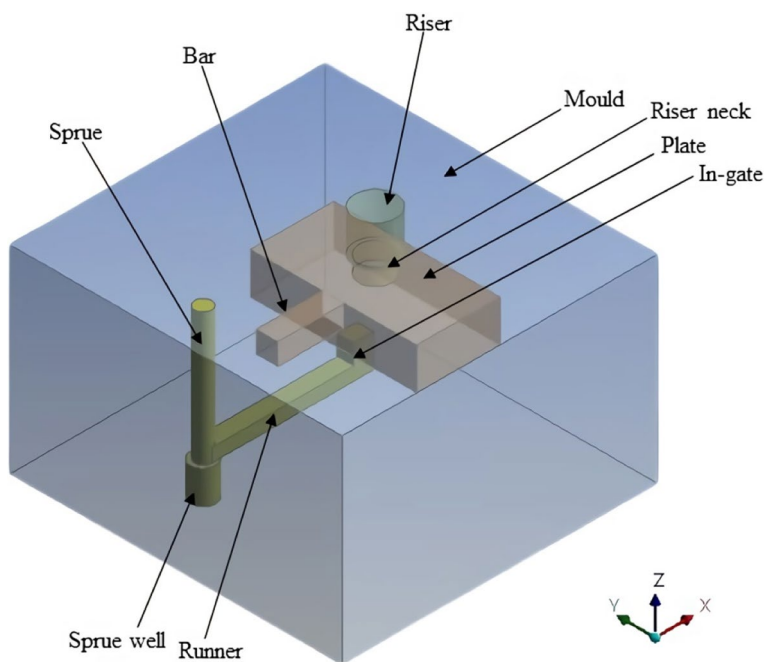


Fig. 1 Bottom gating casting used by Mozammil et al. [15]

Table 1 Dimensions used in bottom gating casting [15]

Name of the components	Name of the parameters	Value (in mm)
Diameter of sprue	Diameter	10
	Length	80
Sprue well	Diameter	15
	Height	20
Runner	Length	90
	Width	8
	Height	10
In-gate	Length	15
	Width	10
	Height	12
Riser	Diameter	25
	Height	25
Riser neck	Diameter	20
	Height	10

0.0077, 0.0086, 0.0090, and 0.0094 at pouring temperatures 970 K, 1000 K, 1050 K, and 1075 K respectively. Figure 3 shows a better agreement of the present simulation results with the experimental results compared to their simulation results.

Simulation of present work

It is validated that the present methods/model closely resembles the practical scenario. Hence, for further investigation, a 60 mm × 60 mm × 10 mm pure aluminium (99.9% pure Al) casting with steel mould was taken as our study for analysis. The

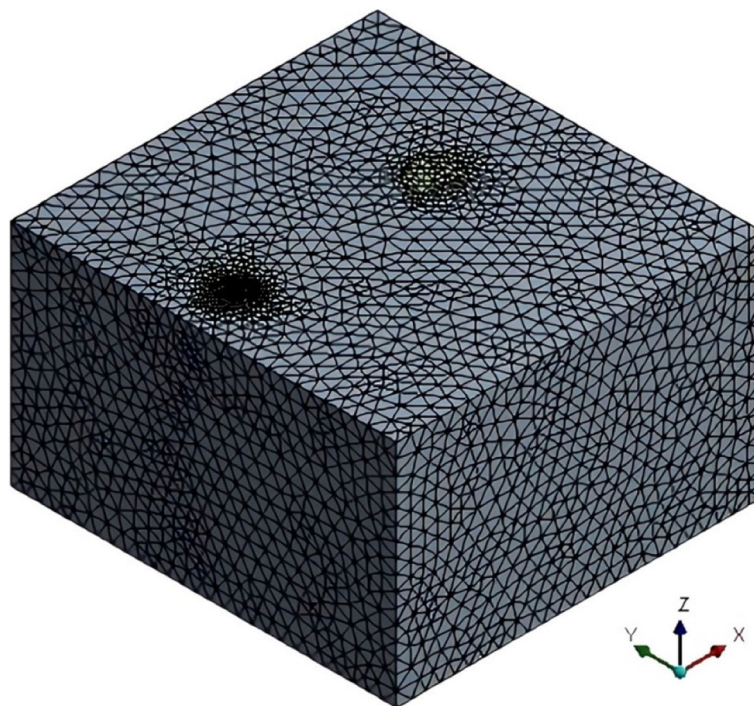


Fig. 2 Mesh view of bottom gating casting

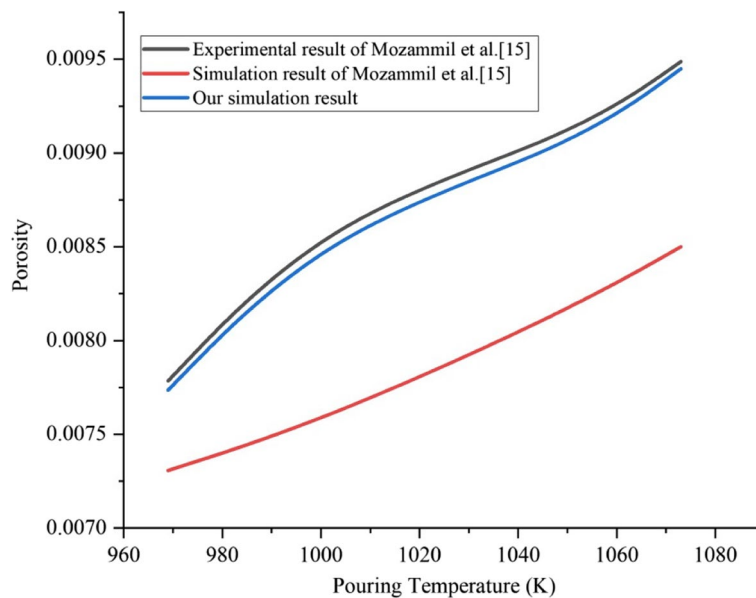


Fig. 3 Comparative analysis of porosity vs pouring temperature

total system of the casting-mould is shown in Fig. 4. This work examines the top gating system because it reduces pouring time as molten metal enters the mould cavity direct from the top. Sprue, riser, mould, casting, and mould wall are illustrated in Fig. 4. A mould cavity or chamber that has been made for the casting where molten metal is poured and solidified. Figure 5 represents the mould cavity for casting and

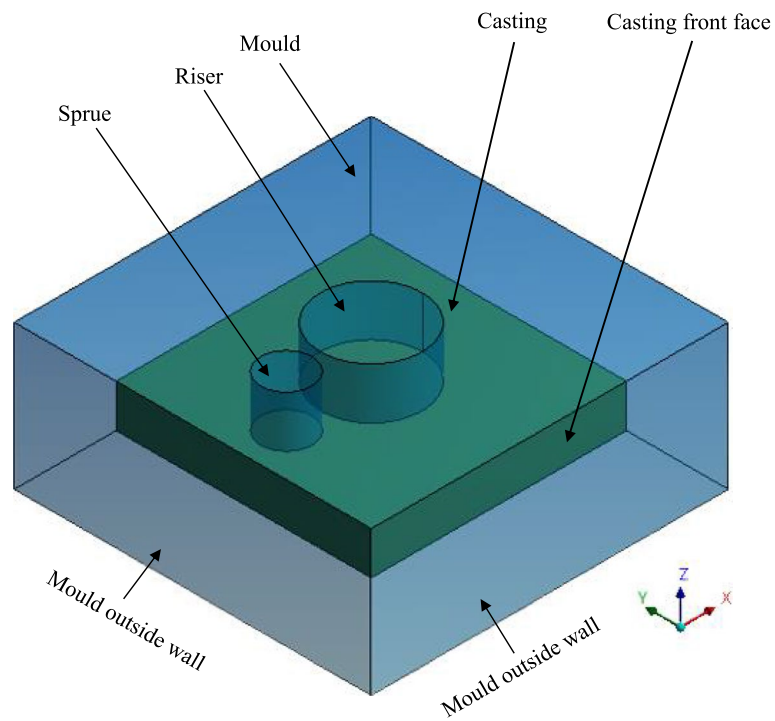


Fig. 4 The mould for present work

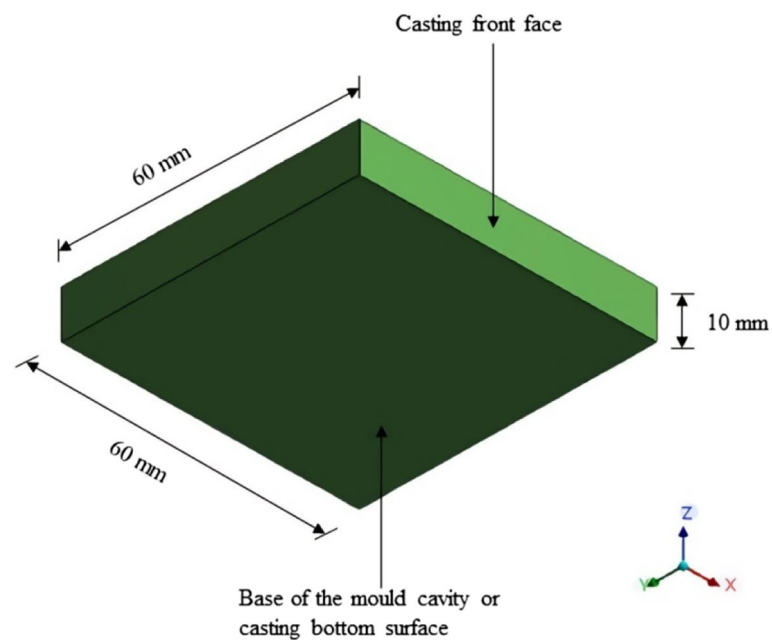


Fig. 5 Dimensions of mould cavity or casting

the cavity's dimensions, which are 60 mm in length, 60 mm in breadth, and 10 mm in depth or thickness. After solidification of the molten aluminium metal, the 60 mm × 60 mm × 10 mm aluminium casting is produced in the mould cavity with

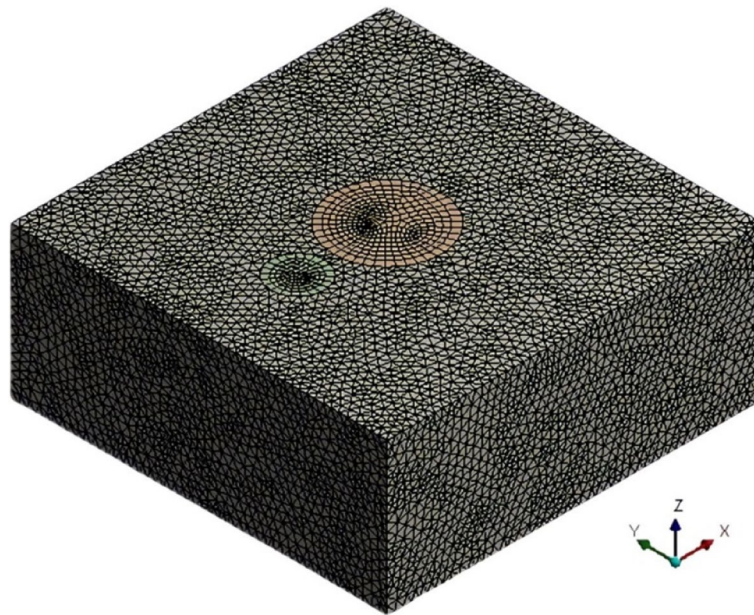


Fig. 6 Mesh in analysed system

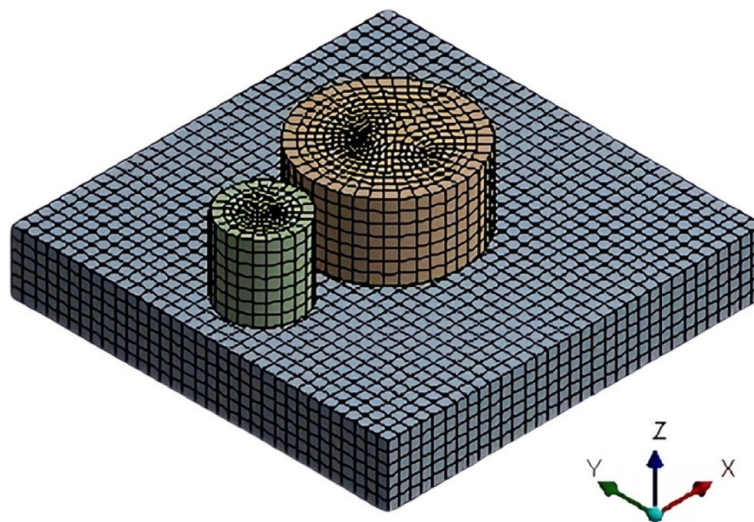


Fig. 7 Mesh in casting, riser, and sprue

or without pores depending on various parameters. The different faces or surfaces and walls are shown in Figs. 4 and 5.

Figures 6 and 7 depict the mesh view of the entire analysed system and the mesh view of the casting, riser, and sprue respectively.

The mould is made of 1.5% carbon steel of dimension $84 \text{ mm} \times 84 \text{ mm} \times 34 \text{ mm}$. The thermophysical properties of aluminium, steel, and air are shown in Table 2 [31, 32]. The riser is placed in the middle of the casting so that it can feed equally in all directions of the casting. The shape and size of the riser are determined by Caine's method [33]. According to Caine's method, the time it takes for solidification to occur is directly

Table 2 Thermo-physical properties of the aluminium, air, and steel used in the simulations

Name	Property	Symbol	Value	Unit
Aluminium	Thermal conductivity (liquid)	k_l	100	W/m K
	Thermal conductivity (solid)	k_s	200	W/m K
	Specific heat (liquid)	C_l	1200	J/kg K
	Specific heat (solid)	C_s	1060	J/kg K
	Density	ρ_{Al}	2690	kg/m ³
	Viscosity	μ_{Al}	0.001	kg/m s
	Freezing temperature	T_f	933	K
	Pure solvent melting heat	L	391	kJ/kg
Air	Thermal conductivity	k_a	0.0336	W/m K
	Specific heat	C_a	1014	J/kg K
	Density	ρ_a	0.8826	kg/m ³
	Viscosity	μ_a	2.286e-05	kg/m s
Steel	Thermal conductivity	k_{st}	33	W/m K
	Specific heat	C_{st}	486	J/kg K
	Density	ρ_{st}	7753	kg/m ³

proportional to the square of the ratio of volume to the surface area. To neglect shrinkage porosity it was taken into account that aluminium experiences a volumetric shrinkage of about 6% during solidification [33].

The analysed system has air filled inside the casting at atmospheric temperature initially. During the filling process, the molten metal enters the mould cavity through the sprue (inflow zone). At the inflow zone, velocity is the same as the pouring velocity of molten metal, and temperature is equal to the pouring temperature of molten metal. In this two-phase system, the primary and secondary phases are air and aluminium respectively. During the pouring process, the air is allowed to leave through the riser (outflow zone). A pressure outlet boundary condition is imposed at the outflow zone (ambient air pressure is specified). Six outside boundary surface walls of the mould are exposed to the atmosphere, where natural convection occurs. The convection heat transfer coefficients are calculated by taking air properties [31] (thermal conductivity, kinematic viscosity, and Prandtl number) at mean film temperature to determine the natural convection between the mould surface wall and atmospheric air. For different Rayleigh number (Ra) ranges, the convection heat transfer coefficient calculation formula has been applied [31].

The Rayleigh number is given by

$$Ra = \frac{gcL^3\rho^2\Delta TPr}{\gamma^2}$$

where ΔT denotes the difference in temperature between the casting surface and atmosphere, γ is the kinematic viscosity of air [m²/s], L is the length of the outside surface of the casting [m], c is the volumetric coefficient of thermal expansion of air [K⁻¹], and Pr is the Prandtl number of air. The convection heat transfer coefficient (denoted by h) [W/m² K] for different types of surface geometry is calculated by the equations given below.

For vertical surfaces,

$$h = \begin{cases} 1.42 \left(\frac{\Delta T}{L} \right)^{1/4}, & \text{where } 10^4 < Ra \leq 10^9 \\ 1.31 (\Delta T)^{1/3}, & \text{where } 10^9 < Ra \leq 10^{13} \end{cases}$$

For upper-heated horizontal surfaces,

$$h = \begin{cases} 1.32 \left(\frac{\Delta T}{L} \right)^{1/4}, & \text{where } 10^5 < Ra \leq 2 \times 10^7 \\ 1.52 (\Delta T)^{1/3}, & \text{where } 2 \times 10^7 < Ra \leq 3 \times 10^{10} \end{cases}$$

For lower-heated horizontal surfaces,

$$h = 0.59 \left(\frac{\Delta T}{L} \right)^{1/4}, \text{ where } 3 \times 10^5 < Ra \leq 3 \times 10^{10}$$

Mesh and mesh sensitivity analysis

The mesh quality influences the convergence and accuracy of the CFD solution. The mesh has been constructed using Ansys-Fluent simulation software. The fine mesh was used in this study to get high accuracy and convergence of the CFD solution. The mesh has a minimum and maximum face area of $1.330285e-08 \text{ m}^2$ and $1.084870e-06 \text{ m}^2$ respectively. The mesh density is higher in the central region of the cylinders (Figs. 6 and 7) because all meshes intersect here.

The mesh sensitivity analysis has been studied. Three types of mesh or grid were chosen: coarse, medium, and fine of their mesh number 19764, 50,956, and 130,276 for the analysis of mesh sensitivity. The coarse, medium, and fine grids are identified by the notations 1, 2, and 3 respectively. The Al volume fraction was measured after 0.4 s for coarse, medium, and fine mesh structures at 983 K pouring temperature and 380 mm/s pouring velocity. The values obtained are 0.3163, 0.3364, and 0.3388, respectively. These values are represented as f_1 , f_2 , and f_3 respectively. The grid convergence index (GCI) has been calculated using Richardson extrapolation methods and is an excellent indicator of discretization uncertainty [21]. The steps for investigating grid convergence are as follows [34].

The order of convergence, oc , is determined by the following equation:

$$oc = \ln \frac{(f_1 - f_2)}{(f_2 - f_3)} / \ln r$$

where r is the grid refinement ratio which is the ratio of the numbers of mesh between two grids. The calculated value of the grid refinement ratio is 2.56.

The relative error (e) between two grids is calculated as

$$e_{1,2} = \left| \frac{f_2 - f_1}{f_2} \right|$$

$$e_{2,3} = \left| \frac{f_3 - f_2}{f_3} \right|$$

The calculated value of relative error for grids 1 and 2 ($e_{1,2}$) is 0.0598 and for grids 2 and 3 ($e_{2,3}$) is 0.0071. The relative error is very small for grids 2 and 3. It is evident

that a mesh value of 50,956 cells or higher will provide a solution that is independent of the mesh size. All of the predicted results in this study have been obtained using a fine mesh.

The following equation is used to calculate the grid convergence index:

$$GCI = \frac{1.25|e|}{r^{oc} - 1}$$

The grid convergence index for grids 1 and 2 ($GCI_{1,2}$) is 0.0101 and for grids 2 and 3 ($GCI_{2,3}$) is 0.0012. The error is 0.0012 or 0.12% for the discretization solution.

It is also important to check whether the solutions are within the asymptotic range of convergence. This can be checked using the following relationship:

$$\frac{GCI_{1,2}}{r^{oc} GCI_{2,3}} \cong 1$$

The value of the left-hand side of the relationship is 1.0071, which is close to one and implies that the solutions are well in the asymptotic range of convergence.

Results and discussion

The methods/model have been applied to the present simulation. In this work, cooling has been done till the maximum temperature of the mould-casting system reaches approximately 430 K (157 °C). Simulations have been carried out using five pouring velocities [in mm/s]: 380, 415, 450, 485, and 520. The liquid metal is poured at temperatures of 983 K (superheat = 50), 1003 K (superheat = 70), and 1033 K (superheat = 100). Thus, simulations for fifteen cases were carried out by varying each pouring temperature with different pouring velocities.

The momentum equation was discretized using the implicit approach as suggested by Calderón-Ramos et al. [35]. The PRESTO [35] scheme was employed for pressure interpolation. The QUICK and compressive schemes were used to solve the energy and VOF equations. The pressure solver SIMPLEC was employed to couple the pressure–velocity variables [35]. To achieve a stable iterative process, under-relaxation factors were employed as stated by Xu et al. [36]. The typical values of under-relaxation factors employed in the study are 0.3 for pressure, 1 for density and body force, 0.7 for momentum, 0.5 for volume fraction, 0.9 for liquid fraction, 0.8 for turbulence quantities, and 1 for energy. At each time step, a lengthy solution has been solved in this study until convergence was obtained as suggested by Nzebuka et al. [21]. A time step of 10^{-5} s is used to initialise the calculation for the temporal convergence of all equations in the simulation. It is later (after 2 s of running the simulation) updated to 10^{-4} s to reduce the overall simulation completion time while maintaining equation convergence. This was done in accordance with Wu et al. [37]. The simulations were conducted on a machine with a Core-i7 processor and 16 GB RAM. Each simulation takes an average of 130 to 150 h to complete.

Solidification and free surface of mould filling process

The solidification and free surface of the filling process are obtained by the 3D simulation model at different times. The middle plane in the casting is taken to represent the filling and solidification process. The middle plane is located on the z - x axis, 30 mm away from the casting's front face along the y -axis as shown in Figs. 4 and 5. The cooling process and flow of liquid metal in the whole simulation of the casting-filling process are described as shown in Fig. 8. These are presented for a pouring velocity of 380 mm/s and a pouring temperature of 983 K. The two-phase system (air and aluminium) and the mixture of two phases with different states (liquid and solid) of aluminium are presented in this study.

- (i) At 0 s the mould cavity is filled by air at ambient temperature. Liquid Al enters the mould cavity from the sprue outlet boundary at 0.1 s as shown in Fig. 8a. The air mixes with liquid Al metal and forms a liquid Al-air layer due to the high solubility of air in molten liquid at a higher temperature. The liquid Al is surrounded by a liquid Al-air mixture layer. At first, the liquid Al-air layer comes in contact with the bottom of the mould cavity as shown in Fig. 8a.
- (ii) After 0.1 s, the molten Al makes contact with the cavity's bottom and left side wall as indicated in Fig. 8b. Some liquid Al solidifies at the left side wall of the cavity, producing a liquid–solid Al mixture. Simultaneously, liquid Al moves to the cavity's right side. The air is displaced as liquid Al filled the area. A liquid Al-air layer is formed around the flow of liquid Al due to the significantly low advective heat transfer coefficient between liquid Al and the air.
- (iii) Around 0.25 s, the liquid aluminium starts to solidify. Before complete solidification, an intermediate phase liquid–solid aluminium mixture forms (Fig. 8b, c). Liquid Al metal continues to flow smoothly into the mould cavity (Fig. 8c). As molten metal travels, the liquid–solid Al mixture layer and liquid Al-air layer shift to the right of the cavity.
- (iv) Liquid metal commences flowing back from the right wall of the mould cavity. The bottom of the cavity is filled with Al metal at around 0.75 s as shown in Fig. 8d. Some liquid metal solidifies from the liquid–solid Al mixture near the bottom right corner, where liquid metal begins to flow back.
- (v) Pouring is done up to 1 s. Most of the Al metal is present in liquid form at this moment, particularly below the sprue as shown in Fig. 8e. Solidification of Al gradually increases with time. When liquid metal reaches the right side of the cavity after travelling some distance it loses flowing velocity. Initially, solidification mainly occurs at this right side of the cavity. A porous solidified area (solid aluminium-air mixture) is formed upon the solidified Al metal. All phases such as liquid aluminium, liquid–solid aluminium mixture, solid aluminium, liquid aluminium-air mixture, solid aluminium-air mixture, and air are present at this time as shown in Fig. 8e.
- (vi) As seen in Fig. 8f, the depth of Al solidified metal is higher at the right and left walls and low in the middle. The riser is placed at the center of the cavity. Some molten aluminium is present in liquid form in the middle of the cavity below the riser. A liquid aluminium-air mixture layer is also formed below the riser. The

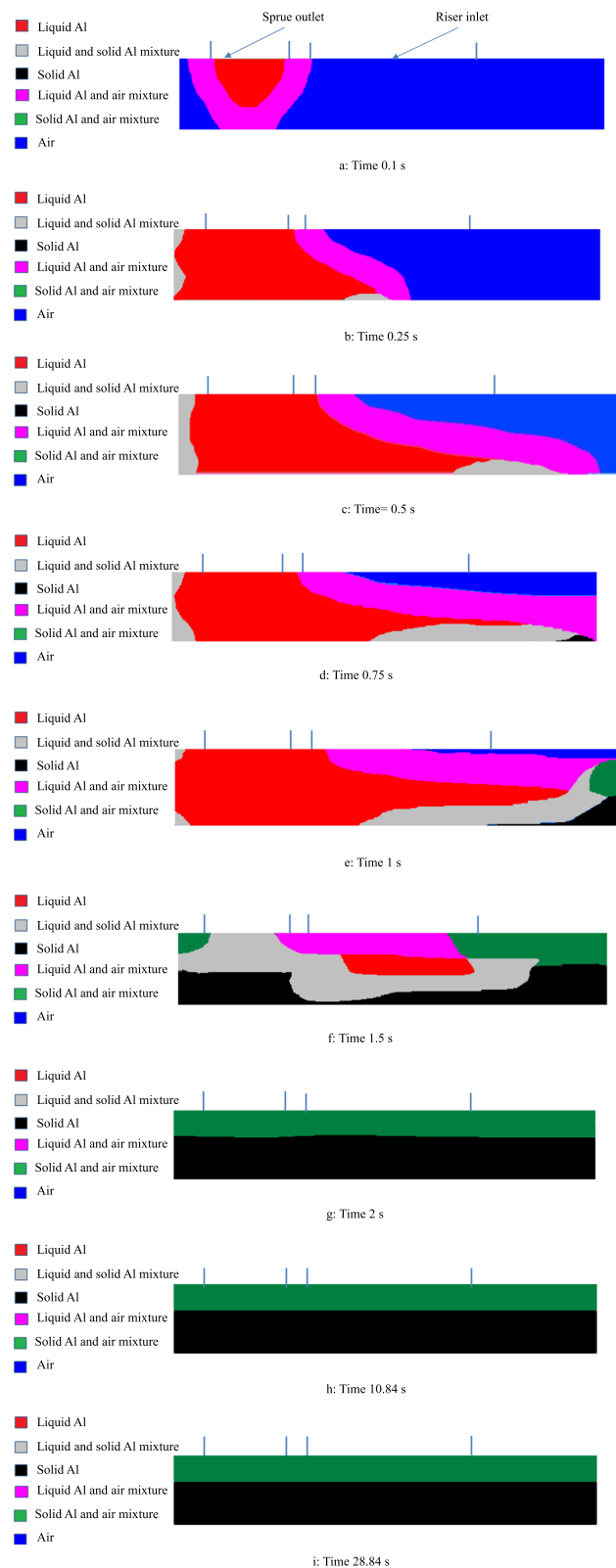


Fig. 8 Simulation of solidification and free surface of mould filling process. **a** Time 0.1 s. **b** Time 0.25 s. **c** Time 0.5 s. **d** Time 0.75 s. **e** Time 1 s. **f** Time 1.5 s. **g** Time 2 s. **h** Time 10.84 s. **i** Time 28.84 s

- porous solidified area (solid aluminium-air mixture) is mainly formed at the upper right portion of the cavity. All phases are present at this time as shown in Fig. 8f.
- (vii) All aluminium liquid metal solidifies about 2 s (Fig. 8g). The temperature is below 933 K everywhere in the casting. Solid aluminium is formed on the lower side of the cavity. The upper side of the cavity has a solid aluminium-air mixture layer.
- (viii) Thus, two layers form in the cavity, one of solid aluminium and the other of the solid aluminium-air mixture. Upon cooling, the layers get small displaced due to volume contraction in the solid metal as shown in Fig. 8h. The cooling is done up to 28.8 s. After about 2 s, no effective change happens in the solidified casting as shown in Fig. 8g, h, and i.

Measurement of porosity and its characteristics

The porosity of the casting was noted at each simulation variant. The variation of porosity with pouring temperature is shown in Fig. 9 and Table 3. At 983 K, the porosity gradually decreases with pouring velocity (Fig. 9). It is seen that at 983 K porosity decreases with a high rate from 0.1706 to 0.0023 when velocity increases from 315 mm/s to 520 mm/s. The decrease rate is around 98.7%. Similarly, at 1003 K, the porosity gradually decreases with pouring velocity, and the decrease rate is around 98.6%. Likewise, to the other pouring temperatures, at 1033 K, the porosity gradually decreases with pouring velocity. When the velocity rises from 315 mm/s to 520 mm/s at 1033 K, porosity decreases considerably with a decrease rate is around 98.7%. Thus, as a result, porosity gradually decreases with pouring velocity for a constant pouring temperature. A similar result was also observed from the work of Xu et al. [38]. Their research [38] showed that porosity could be minimised to 0.9% by increasing injection velocity, with the minimum porosity being achieved at 0.7 m/s of Al alloy. The

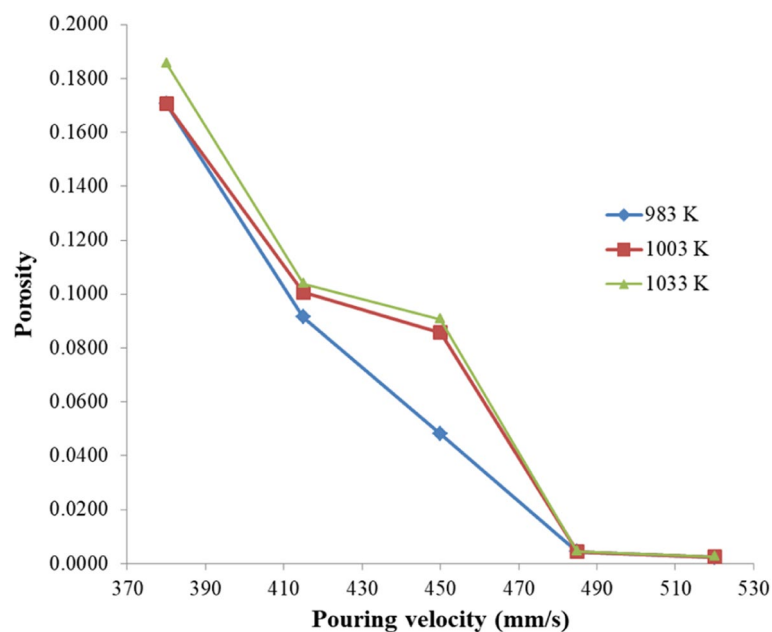


Fig. 9 Variation of porosity with pouring velocity at different pouring temperatures

Table 3 Solid aluminium filled from the base of the mould cavity at different pouring parameters

Pouring temperature (K)	Pouring velocity (mm/s)	Length of fully filled solidified Al from the base of the mould cavity (mm)	Percentage of the length of fully filled solidified Al from the base of the mould cavity	Porosity
983	380	6.5	65	0.1706
	415	6.7	67	0.0914
	450	7.7	77	0.0481
	485	10.0	100	0.0044
	520	10.0	100	0.0023
1003	380	6.3	63	0.1706
	415	6.5	65	0.1007
	450	6.9	69	0.0858
	485	10.0	100	0.0044
	520	10.0	100	0.0024
1033	380	6.1	61	0.1854
	415	6.4	64	0.1038
	450	6.8	68	0.0906
	485	10.0	100	0.0045
	520	10.0	100	0.0024

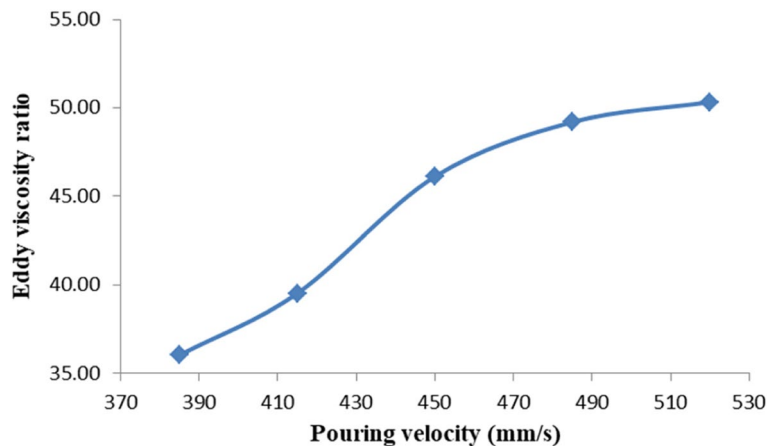


Fig. 10 Eddy viscosity ratio variation with pouring velocity

porosity decreases due to the increase in the turbulence of flow in the cavity as the pouring velocity increases. As turbulence increases, the trapped air escapes from the metal which reduces the porosity.

The turbulence eddy viscosity ratio has been drawn with pouring velocity in Fig. 10 at 983 K pouring temperature. It is seen from Fig. 10 that the level of turbulence (turbulence eddy viscosity ratio) increases with pouring velocity. This study of the eddy viscosity ratio was observed in the work of Nzebuka et al. [21] and Waheed et al. [27]. However, in their work [21, 27], they studied the variation of turbulence eddy viscosity ratio with distance from the inlet.

At 380 mm/s velocity (Fig. 9 and Table 3), porosity is almost constant over the temperature range of 983 K to 1003 K and beyond that, it increases with temperature. The porosity also increases with temperature at a pouring velocity of 415 mm/s. The porosity increases at a slow rate from about 9 to 10% when the pouring temperature reaches 983 K to 1033 K at a pouring rate of 415 mm/s (Fig. 9). The summary of results is depicted in Table 4 where the percentage of increase of fully solidified aluminium filled from the base of the mould cavity and the percentage of decrease of porosity with superheat are presented.

Similarly, the porosity rises with pouring temperature at a pouring velocity of 450 mm/s (Fig. 9 and Table 3). The result demonstrates that, at 485 mm/s velocity, the porosity is almost constant over the temperature range 983 K to 1003 K, and beyond that, it increases when pouring temperature up to it reaches 1033 K. At a pouring rate of 485 mm/s, the porosity is very low (about 0.4%) and nearly constant as the pouring temperature rises. At 520 mm/s velocity, porosity increases with pouring temperature from 983 to 1003 K, then remain almost constant up to 1033 K. The porosity is very small at 520 mm/s of pouring rate and it is just around 0.2% throughout the range of 983 K to 1033 K. It is observed that the porosity value is found to be extremely low for velocities of 485 mm/s and 520 mm/s, and the porosity is nearly constant whatever the pouring temperature.

Thus, as a result, porosity is almost constant in a certain range of temperature or increases with increasing temperature for a constant velocity (380 mm/s, 485 mm/s, and 520 mm/s). Where Mozammil et al. [15] and Jahangiri et al. [39] established that porosity increases with increasing pouring temperature. The present study observed that it is not always true and there might be certain ranges of temperatures where the porosity remains constant or nearly constant with increasing pouring temperature. It is observed that for the pouring velocities 380 mm/s, 485 mm/s, and 520 mm/s, porosity increases with pouring temperature when the range of temperature is large. Thus it can be concluded that porosity increases with pouring temperature, but the rate of increase is quite slow. Porosity usually appears in the cast metal area due to the high solubility of air in Al at higher temperatures. Air solubility increases with increasing pouring temperature and results in increased porosity.

Porosity decreases when the pouring temperature decreases and the pouring velocity increases. The rate of decrease in porosity is low with decreasing pouring temperature but is quite high with increasing pouring velocity. Hence, it can be concluded that porosity has little dependence on pouring temperature rather than pouring velocity.

Table 4 Variation of solid aluminium filled from the base of cavity and porosity

Pouring temperature (K)	Percentage of superheat increase	Percentage increase of fully filled solidified Al length from the base of mould cavity from velocity 380–520 mm/s	The percentage of porosity decreased from a velocity 380–520 mm/s
983	5.4	53.85	98.6
1003	7.5	58.73	98.6
1033	10.7	63.93	98.7

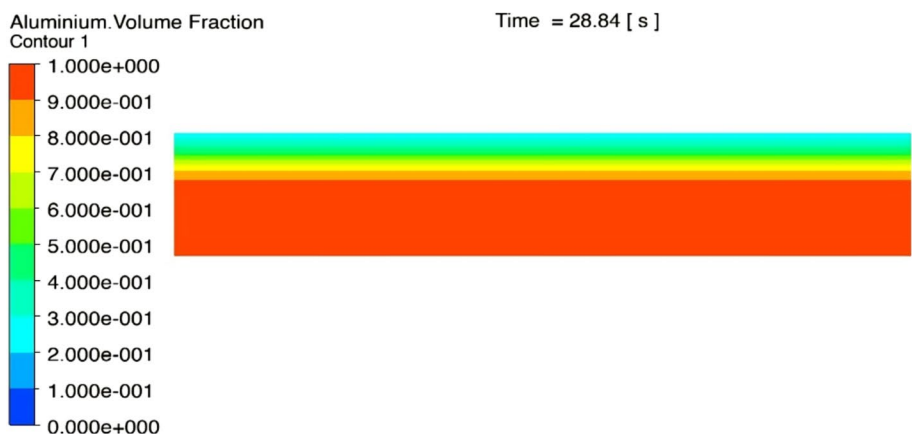
After measuring the porosity, its nature has been observed in this study. It is also necessary to have an idea of how much thickness of casting with no pores or a negligible pore (i.e., filled by about 100% Al metal) is produced in a finished casting for various casting parameters. To compute the aforementioned measurement the contours of the Al volume fraction are generated for different planes in the casting domain. Three cross-sectional planes are chosen on the z - x plane to draw the volume fractions of aluminium. The first plane is the front face of the casting. The front face of the casting is located in the z - x plane as shown in Figs. 4 and 5. The second plane lies on the z - x plane, 15 mm away from the casting's front face along the y -axis. The third plane is in the middle of the casting, i.e., is located on the z - x plane, 30 mm away from the casting's front face along the y -axis. Since simulation has been performed up to a maximum temperature of roughly 430 K (157 °C) of the whole cast-mould system and the corresponding time to reach this temperature is shown in the contours obtained for every simulation. The contours of the aluminium volume fraction at pouring velocity 380 mm/s and pouring temperature 983 K are given in Fig. 11.

Figure 11a–c shows that the aluminium volume fraction is reducing while approaching the top of the cavity. This is expected as air is moving towards the top and escaping through the riser. The figures also show almost similar distribution over the whole cavity. The contour of volume fraction was also noticed in the centrifugal casting as revealed in the work of Thomas et al. [40]. They [40] measured the concentration of particles through the contour of volume fraction.

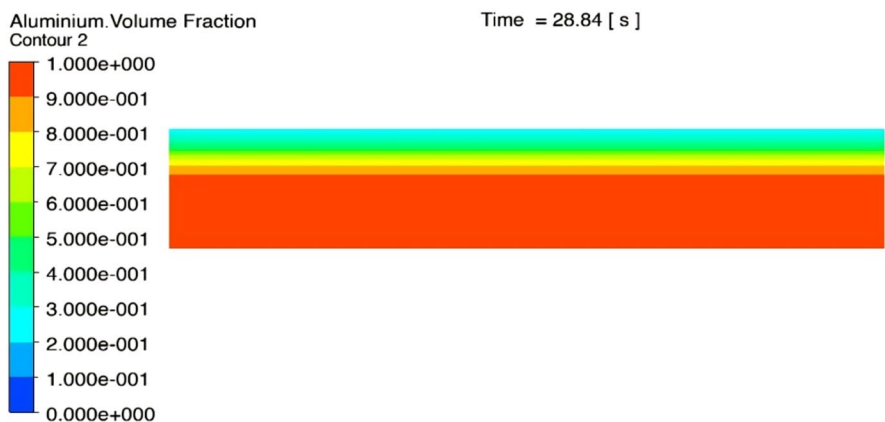
It has been verified that the contours of the Al volume fraction are the same on any z - x plane for various values of y for a given specific set of casting conditions. The contours of the Al volume fraction for others pouring parameter combinations are also studied. According to the generalized observations, the percentage of porosity increases from almost zero value (adjacent to the 100% Al existing) to maximum value along the thickness of the casting. It achieves its highest value at the casting's top surface. Figure 11 shows that some air is entrapped during the solidification of casting, creating porosity in the casting. Porosity is mostly found on the casting's top surface as in Fig. 11 where dark red fill colour implies around 100% Al volume fraction which is in good agreement with Cao et al. [14]. The top surface of the casting has 70% of the overall porosity (Fig. 11). According to Fig. 8, after solidification two layers are formed in the solidified casting, one of pure solid aluminium and the other of the solid aluminium-air mixture. This solid aluminium-air combination layer is mainly responsible for the formation of porosity.

Table 3 and Fig. 12 depict the variation in the length of solidified Al filled from the base of the mould cavity (mm) at different pouring parameters. The length of solidified aluminium (approximately 100% Al) from the base of the cavity gradually increases with pouring velocity for a constant pouring temperature and it increases with decreasing pouring temperature for a constant pouring velocity. As the porosity decreases with increasing pouring velocity, therefore this filling length from the base of the mould cavity also increases. Similarly, due to the porosity decreasing with decreasing pouring temperature for a constant pouring velocity, this length increases.

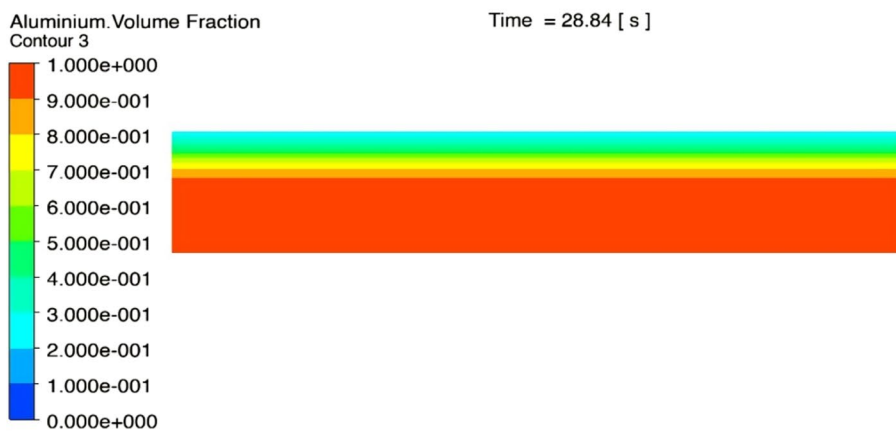
As per Fig. 12, about 100% Al fill in the entire mould cavity at 485 mm/s, and 520 mm/s as there is almost no porosity. It shows that for pouring velocities of 485 mm/s and 520 mm/s, almost porous free casting has been found. Thus, from



a: At first plane.



b: At second plane.



c: At third plane

Fig. 11 Contours of aluminium volume fraction at 380 mm/s and 983 K. **a** At first plane. **b** At second plane. **c** At third plane

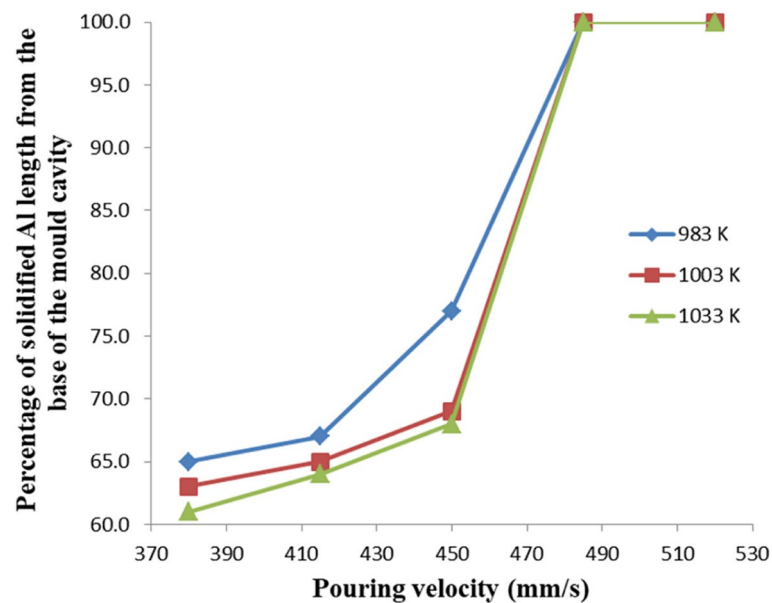


Fig. 12 Variation of solidified Al length from the base of mould cavity

observations likely that 100% aluminium filling happens in the mould cavity at near the pouring velocity of 500 mm/s. The 100% aluminium-filled length in the mould cavity increases with pouring velocity and gets a maximum value near 500 mm/s. At a pouring velocity of 380 mm/s, the mould cavity can be seen to fill with even less than 50% aluminium at the upper surface. If the pouring velocity is too slow, the metal will freeze before filling the mould cavity and lower velocities will mean that the percentage of aluminium will decrease. On the other hand, a high pouring velocity is not feasible because turbulence may result in defects like gas bubbles at high-speed [15]. Pouring velocity is determined by the height of the pouring basin [33]. The more pouring velocity means more pouring basin height which increases the initial cost. So, an optimal pouring velocity must be maintained. From the present study, it can be concluded that the optimal pouring velocity is near 500 mm/s. The porous free casting has been found at a near pouring velocity of 500 mm/s.

High porosity in the casting occurs as a result of high pouring temperature (Table 3) which results in poor strength in the casting. Low pouring temperature decreases the fluidity of the molten metal. In this simulation pouring temperatures of 983 K, 1003 K, and 1033 K were used and it is seen that the length of fully aluminium-filled in the mould cavity increases with decreasing pouring temperature.

Conclusions

The parameters relating to the porosity defect that impacts casting quality were investigated. The optimal pouring velocity is near 500 mm/s. When the velocity is close to 500 mm/s, it is seen that the porosity value is extremely low, and the porosity is almost constant regardless of the pouring temperature. The length of fully filled solid Al from the base of the mould cavity rises with pouring velocity and reaches its

maximum value close to 500 mm/s. Additionally, this length gradually increases with decreasing pouring temperature for a constant pouring velocity.

After solidification, two layers are formed in the solidified casting, one of pure solid aluminium and the other of the solid aluminium-air mixture. This solid aluminium-air combination layer is responsible for porosity formation. The porosity gradually decreases with increasing pouring velocity for a fixed pouring temperature. The porosity is almost constant to a certain extent of temperature or gradually increases with increasing pouring temperature for a fixed pouring velocity. A pouring temperature of 983 K showed the best results for getting low porous casting. Porosity has little dependence on pouring temperature rather than pouring velocity. The percentage of porosity increases from zero value (adjacent to the 100% Al existing) to maximum value along the thickness of the casting. It achieves its highest value at the casting's top surface.

The research may be extended in the future to study the optimization of casting parameters for other defects in similarly related model analysis.

Abbreviations

Al	Aluminium
CFD	Computational fluid dynamics
VOF	Volume of fluid
St	Steel
ref	Reference
a	Air
Ansys	Analysis of systems
Ansys Fluent	Fluid simulation software
RNG	Renormalization group
k-ε	K-epsilon model for turbulence flow
GB	Gigabytes
RAM	Random-access memory

Acknowledgements

Not applicable.

Authors' contributions

This article is part of the Ph.D. work of SC. The PhD work was supervised by SS at Jadavpur University, Kolkata. The authors have read and approved the final manuscript.

Funding

This research acquired no explicit funding from any government, commercial, or non-profit organisation.

Availability of data and materials

The data acquired and/or evaluated during the present research are accessible upon valid request from the corresponding author.

Declarations

Competing interests

The authors confirm that they do not have competing interests.

Received: 29 November 2022 Accepted: 9 March 2023

Published online: 23 March 2023

References

1. Tiryakioğlu M, Yousefian P, Eason PD (2018) Quantification of entrainment damage in a356 aluminum alloy castings. *Metallurgical Mater Trans A* 49(11):5815–5822
2. Zhang S, Xu Z, Wang Z (2017) Numerical modeling and simulation of water cooling-controlled solidification for aluminum alloy investment casting. *Int J Adv Manufact Technol* 91(1):763–770
3. Souissi N, Souissi S, Le Niniven C, Amar MB, Bradai C, Elhalouani F (2014) Optimization of squeeze casting parameters for 2017 a wrought Al alloy using Taguchi Method. *Metals* 4(2):141–154
4. Chudasama BJ (2013) Solidification analysis and optimization using Pro-cast. *Int J Res Modern Eng Emerg Technol* 1(4):9–19

5. Ayar MS, Ayar VS, George PM (2020) Simulation and experimental validation for defect reduction in geometry varied aluminium plates casted using sand casting. *Mater Today: Proc* 27:1422–1430
6. Hirata N, Anzai K (2017) Numerical simulation of shrinkage formation behavior with consideration of solidification progress during mold filling using stabilized particle method. *Mater Trans* 58(6):932–937
7. Bekele BT, Bhaskaran J, Tolcha SD, Gelaw M (2022) Simulation and experimental analysis of re-design the faulty position of the riser to minimize shrinkage porosity defect in sand cast sprocket gear. *Mater Today: Proc* 59:598–604
8. Choudhari CM, Narkhede BE, Mahajan SK (2014) Casting design and simulation of cover plate using AutoCAST-X software for defect minimization with experimental validation. *Proc Mater Sci* 6:786–797
9. Böllinghaus T., Herold H., Cross C.E., Lippold J.C. (2008) Hot cracking phenomena in welds II. Springer ebook collection / Chemistry and Materials Science 2005–2008. Springer, Berlin Heidelberg
10. Nazarboland A, Elliott R (1997) The effect of intrinsic casting defects on the mechanical properties of austempered, alloyed ductile iron. *Int J Cast Met Res* 10(2):87–97
11. Bonollo F, Gramegna N, Timelli G (2015) High-pressure die-casting: contradictions and challenges *Jom* 67(5):901–908
12. Bhagavath S, Cai B, Atwood R, Li M, Ghaffari B, Lee PD, Karagadde S (2019) Combined deformation and solidification-driven porosity formation in aluminum alloys. *Metall and Mater Trans A* 50(10):4891–4899
13. Chakravarti S, Sen S, Bandyopadhyay A (2018) A study on solidification of large iron casting in a thin water cooled copper mould. *Mater Today: Proc* 5(2):4149–4155
14. Cao H, Shen C, Wang C, Xu H, Zhu J (2019) Direct observation of filling process and porosity prediction in high pressure die casting. *Materials* 12(7):1099
15. Mozammil S, Karloopia J, Jha PK (2018) Investigation of porosity in Al casting. *Mater Today: Proc* 5(9):17270–17276
16. Papanikolaou M, Saxena P, Pagone E, Salonitis K, Jolly M. (2020). Optimisation of the filling process in counter-gravity casting. In: IOP Conference Series: Materials Science and Engineering, vol. 861. Bristol: IOP Publishing; p 012031.
17. Jolly M, Katgerman L (2022) Modelling of defects in aluminium cast products. *Prog Mater Sci* 123:100824
18. Namchanthra S, Suvanjumrat C, Chookaew W, Wijitdamkerng W, Promtong M (2022) A CFD investigation into molten metal flow and its solidification under gravity sand moulding in plumbing components. *GEOMATE J* 22(92):100–108
19. Waheed M, Nzebuka G (2020) Analysis of thermally driven flow pattern formation in aluminium DC casting for different Rayleigh numbers and Billet diameters. *Thermal Sci Eng Prog* 18:100536
20. Waheed M, Nzebuka G (2020) Investigation of macrosegregation for different dendritic arm spacing, casting temperature, and thermal boundary conditions in a direct-chill casting. *Appl Phys A* 126:1–12
21. Nzebuka GC, Ufodike CO, Egole CP (2021) Influence of various aspects of low-Reynolds number turbulence models on predicting flow characteristics and transport variables in a horizontal direct-chill casting. *Int J Heat Mass Transf* 179:121648
22. Eqal AK, Yagoob JA et al (2021) Prediction of the solidification mechanism of ZA alloys using Ansys fluent. *J Appl Sci Eng* 24(5):699–706
23. Sowa, L, Skrzypczak T, Kwiaton P (2020) Impact of metal pouring parameters on basic physical processes. *Acta Physica Polonica, A* 138(2):210–13.
24. Skrzypczak T, Węgrzyn-Skrzypczak E, Sowa L (2018) Numerical modeling of solidification process taking into account the effect of air gap. *Appl Math Comput* 321:768–779
25. Tota PV (2009) Turbulent flow over a backward-facing step using the RNG k-ε model. *Flow Sci* 1:1–15
26. Wu Y, Liu Z, Li B, Gan Y (2022) Numerical simulation of multi-size bubbly flow in a continuous casting mold using population balance model. *Powder Technol* 396:224–240
27. Waheed MA, Nzebuka GC, Enweremadu CC (2020) Potent turbulence model for the computation of temperature distribution and eddy viscosity ratio in a horizontal direct-chill casting. *Numerical Heat Transfer, Part A: Appl* 79(4):294–310
28. ANSYS (2014) Ansys fluent user's guide. Fluent, Lebanon
29. Shepel SV, Paolucci S (2002) Numerical simulation of filling and solidification of permanent mold castings. *Appl Therm Eng* 22(2):229–248
30. Campbell J (2015) Complete casting handbook: metal casting processes, metallurgy, techniques and design. Elsevier Science, New York. <https://books.google.co.in/books?id=4HhYrgEACAAJ>
31. Özışık MN (1985) Heat transfer: a basic approach. heat transfer: a basic approach. McGraw-Hill, New York. <https://books.google.co.in/books?id=Jm-fPwAACAAJ>
32. Conde R, Parra MT, Castro F, Villafrauela JM, Rodriguez M, Méndez C (2004) Numerical model for two-phase solidification problem in a pipe. *Applied Therm Eng* 24(17–18):2501–2509
33. Ghosh A, Mallik AK (1986) Manufacturing Science. Ellis Horwood series in Engineering Science. Ellis Horwood, United Kingdom. https://books.google.co.in/books?id=_5-QgAACAAJ
34. Roache PJ (1994) Perspective: a method for uniform reporting of grid refinement studies. *J Fluids Eng* 116(3):405–413. <https://doi.org/10.1115/1.2910291>
35. Calderón-Ramos I, Morales RD, Servín-Castañeda R, Pérez-Alvarado A, García-Hernández S, de Jesús Barreto J, Arreola-Villa SA (2019) Modeling study of turbulent flow in a continuous casting slab mold comparing three ports SEN designs. *ISIJ Int* 59(1):76–85
36. Xu M, Isac M, Guthrie RI (2018) A numerical simulation of transport phenomena during the horizontal single belt casting process using an inclined feeding system. *Metall Mater Trans B* 49:1003–1013
37. Wu M, Ahmadein M, Ludwig A (2018) Premature melt solidification during mold filling and its influence on the As-cast structure. *Front Mech Eng* 13:53–65
38. Xu C, Zhao J, Guo A, Li H, Dai G, Zhang X (2017) Effects of injection velocity on microstructure, porosity and mechanical properties of a Rheo-Diecast Al-Zn-Mg-Cu aluminum alloy. *J Mater Process Technol* 249:167–171

39. Jahangiri A, Marashi S, Mohammadaliha M, Ashofte V (2017) The effect of pressure and pouring temperature on the porosity, microstructure, hardness and yield stress of AA2024 aluminum alloy during the squeeze casting process. *J Mater Process Technol* 245:1–6
40. Thomas H., Samad A., Arun MS (2022) Particle distribution simulation of functionally graded Az91-Sicp composite fabricated by centrifugal casting. (Available at SSRN 4295526)

Submit your manuscript to a SpringerOpen[®] journal and benefit from:

- ▶ Convenient online submission
- ▶ Rigorous peer review
- ▶ Open access: articles freely available online
- ▶ High visibility within the field
- ▶ Retaining the copyright to your article

Submit your next manuscript at ▶ [springeropen.com](https://www.springeropen.com)
